Surface Rebound of Relativistic Dislocations Directly and Efficiently Initiates Deformation Twinning

Qing-Jie Li,[1] Ju Li,[2,*] Zhi-Wei Shan,[3,†] and Evan Ma[1,‡]
[1]*Department of Materials Science and Engineering, Johns Hopkins University, Baltimore, Maryland 21218, USA*
[2]*Department of Nuclear Science and Engineering and Department of Materials Science and Engineering, Massachusetts Institute of Technology, 77 Massachusetts Avenue, Cambridge, Massachusetts 02139, USA*
[3]*Center for Advancing Materials Performance from the Nanoscale (CAMP-Nano) & Hysitron Applied Research Center in China (HARCC), State Key Laboratory for Mechanical Behavior of Materials, Xi'an Jiaotong University, Xi'an 710049, China*
(Received 24 June 2016; revised manuscript received 19 August 2016; published 11 October 2016)

Under ultrahigh stresses (e.g., under high strain rates or in small-volume metals) deformation twinning (DT) initiates on a very short time scale, indicating strong spatial-temporal correlations in dislocation dynamics. Using atomistic simulations, here we demonstrate that surface rebound of relativistic dislocations directly and efficiently triggers DT under a wide range of laboratory experimental conditions. Because of its stronger temporal correlation, surface rebound sustained relay of partial dislocations is shown to be dominant over the conventional mechanism of thermally activated nucleation of twinning dislocations.

DOI: 10.1103/PhysRevLett.117.165501

Recent advances in small-volume materials fabrication have created a remarkable category of metallic crystals that can retain pristine crystal structures on the length scale of $10^1 - 10^2$ nanometers [1–7]. Deformation twinning (DT) has been shown to initiate in these metals at ultrahigh stresses ($\sim 10^{-2}G$, where G is shear modulus) and on a very short time scale ($\ll 0.01$ s, the typical time resolution of state-of-the-art *in situ* microscopy imaging techniques) [2,4–6], indicating strong spatial-temporal correlations in the underlying dislocation dynamics. Such strongly correlated DT mode requires extremely stringent spatial and temporal coordination of twinning dislocations (the right type of partial dislocations on *consecutive* atomic planes one after another [8]). This is hardly possible by the conventional pole mechanism [9,10] due to the pristine nature of the deformation volume, nor by the generally believed thermally activated nucleation (TAN) [2,5–7,11–13] due to possible long waiting time.

In the following, we illustrate that while the first dislocation to initiate DT must come from a TAN event, subsequent twinning dislocations can be generated by dislocations running at speeds near the transverse sound speed (c_t). Specifically, twinning dislocations are generated successively on each and every consecutive atomic plane by a surface-rebound sustained (SRS) nucleation process, in a domino cascade fashion. This mechanism is highly efficient due to its strong temporal correlation; i.e., there is almost no time delay between two successive twinning partials. The SRS mechanism can thus dominate over the TAN mechanism over a wide range of experimental conditions.

Atomistic simulations, reaction pathway sampling method, and the harmonic transition state theory will be combined to reveal the mechanism underlying the strongly correlated DT. Direct molecular dynamics (MD) simulations were performed to observe how dislocations behave after nucleation in highly stressed nanowires and slab configurations. The free end nudged elastic band method (FENEB) [11,14] was used to obtain the activation energy barriers for TAN of surface dislocation. The empirical potential for copper [15] based on the embedded atom method was used to describe the interatomic interactions. All simulations were performed using the LAMMPS package [16] and the results were visualized by the AtomEye [17] and DXA packages [18]. See Ref. [19] for more details on simulation methods.

Figure 1 shows DT initiation in MD simulation of a 10 nm wide [100] oriented square nanowire compressed at 300 K with a strain rate of 10^6 s^{-1} (0.0 ps). The first dislocation was nucleated when the sample-wide axial stress reached ~2.5 GPa [21], and glided across the nanowire (5.5 ps). However, instead of TAN of twinning dislocations, the subsequent DT proceeded via repeated surface rebounds. Specifically, when an incident partial dislocation impacted on a free surface and annihilated, new partial dislocations were *immediately* generated (5.5 → 8.0 ps). The new partials are on neighboring slip planes because of the lack of $\mathbf{b}_p \leftrightarrow -\mathbf{b}_p$ symmetry on the same slip plane (the atoms in the two atomic layers would otherwise sit or slide on top of each other) in face-centered cubic (fcc) metals. The rebounded partials are thus naturally twinning dislocations, which are then accelerated again to high speeds under τ, towards the surface on the other side of the sample (12.0 ps), where another collision kicks out more twinning partials that continue the relay (14. 0 ps). Such SRS relay continued until the sample-wide axial stress (σ) was relaxed to a much lower level of 0.75 GPa (17.0 → 60.0 ps) [21]. The whole DT initiation process was accomplished within 60 ps with a 9-layers twin nucleus (60.0 ps). See Ref. [22] for more details and Ref. [23] for similar DT initiation in a [110] oriented

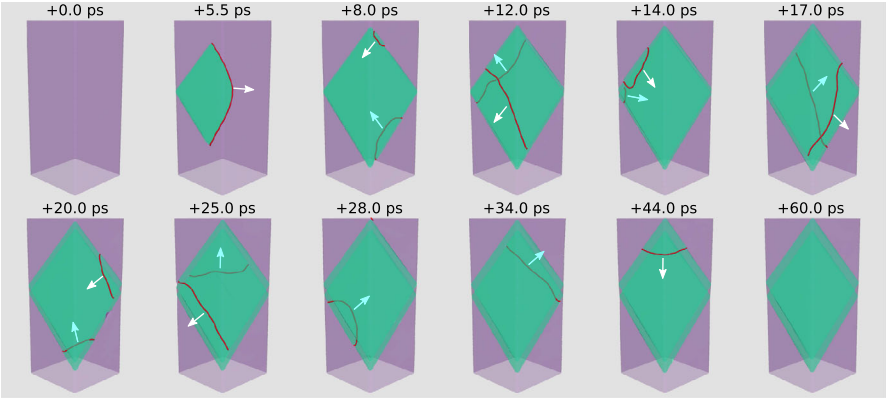

FIG. 1. DT initiation in a [100] oriented square Cu nanowire via surface rebound process. The starting time for DT initiation is 53.858 ns (i.e., +0.0 ps). Red lines are partial dislocation cores, green planes are stacking faults or twin boundaries and short arrows represent directions of dislocation motion.

nanowire under tensile loading. This fascinating observation invites two important questions. First, what is the physical origin of the observed surface rebound? Second, exactly how DT is initiated under typical laboratory and MD simulation conditions, i.e., is this SRS mechanism favored over the TAN mechanism? In what follows, we first rationalize the observed surface rebound and then elucidate the strongly correlated DT initiation process.

MD simulations showed that, under sufficiently high shear stress τ, dislocations can be accelerated to become [24], or even directly born as [25] "relativistic dislocations." As shown in Fig. 2, a partial dislocation was accelerated under an applied τ of 1.55 GPa (typical in laboratory experiments on dislocation-free samples [1,26]) at 2 K. Although being dragged by free surface, the front of a partial dislocation loop was still accelerated to a speed as high as $\sim 0.84 c_t$ and within a distance as short as ~20 nm. Phonon drag has minor effects on this acceleration [27]. As such, dislocations can conceivably enter the kinetic energy dominated, i.e., strongly overdriven, regime in highly stressed pristine crystals.

A dislocation becomes relativistic when the kinetic energy E_k associated with the core becomes equally important as the potential energy E_p ($E_{\text{core}} = E_p + E_k$), and no longer negligible for dislocation reactions [28–31]. When a dislocation with speed v hits a surface, E_{core} must dissipate into heat and transform into new defects (e.g., slip offset, point defects, and mostly M new dislocations). Energy conservation requires

$$E_p(v) + E_k(v) = E_{\text{config}} + \int R_D dt + H(v - v_c) \times \sum_{i=1}^{M} \int R_i dt, \quad (1)$$

where E_{config} is the potential energy of the local configuration due to dislocation annihilation (e.g., a surface slip step), R_D is the dissipation rate into heat, R_i is the transformation rate of E_{core} into the potential energy of ith dislocation, and $H(v - v_c)$ is the Heaviside step function to account for the sharp transition from annihilation to rebound once the dislocation speed v exceeds a critical value v_c.

For $v \ll v_c$, E_k is negligible and there is little new dislocation generation, so $E_{\text{core}} \sim E_p \sim E_{\text{config}} + \int R_D dt$, leading to normal annihilation. For $v > v_c$, the extra E_k feeds into $\int R_D dt + \sum_{i=1}^{M} \int R_i dt$ and the competition between R_D and R_i determines how the system evolves. In our model, defect generation is favored because it involves localized bond breaking which is more efficient than dissipation into heat via elastic bond vibrations, i.e.,$E_k \sim \sum_{i=1}^{M} \int R_i dt$. For a successful dislocation nucleation, the critical (saddle) configuration has to be reached, requiring $\sum_{i=1}^{M} \int R_i dt \geq \sum_{i=1}^{M} Q_i$, where Q_i is the activation barrier (free energy) for dislocation i. Thus for a single rebound, it is necessary that

$$E_k(v) \geq Q \quad \text{and} \quad R_1 \gg R_D. \quad (2)$$

This criterion suggests that once a dislocation accelerates to a critical speed such that its kinetic energy more than compensates for the Q of surface dislocation, the latter nucleates, provided that the dissipation of core energy into heat is insignificant over the very short time period for nucleation.

Our analyses based on the FENEB method and direct MD simulations lend support to Eq. (2). In Fig. 3, using a

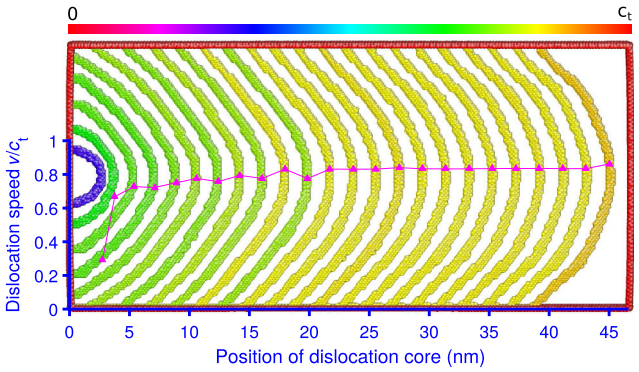

FIG. 2. Trajectory of a partial dislocation being accelerated in a copper slab subjected to a shear stress $\tau \sim 1.55$ GPa at 2 K. The dislocation line is colored corresponding to its instantaneous speed. The crystals directions are $[\bar{1}10]$, $[11\bar{2}]$, and [111] along the dislocation motion direction, the tangent of dislocation front and the slip plane normal.

copper slab under shear stresses τ, $E_k(\tau)$ is compared with the $Q_0(\tau)$, i.e., the Q at 0 K, of a twinning dislocation (after the first leading partial annihilates and leaves behind a stacking fault). In Fig. 3(a), the dislocation core carrying the necessary kinetic energy is identified using the common neighbor analysis (CNA) [32,33]. Atoms right above and below the CNA core are included [Fig. 3(b)] as the rebound process involves these two additional atomic layers. Such a choice of core region to evaluate the necessary E_k is based on the localized nature of dislocation nucleation at the site where a high-speed dislocation hits the surface [34]. $Q_0(\tau)$ is obtained using the FENEB method (see Ref. [35]). A typical saddle configuration for surface dislocation nucleation is shown in Fig. 3(c), which suggests an approximately semicircular shape involving two atomic planes. The results can be expressed as [Fig. 3(d)] $Q_0(\tau) = A\{1 - \exp[\alpha(1 - \tau/\tau_0)]\}$ [12], where A, α, and τ_0 are fitting parameters. This enables us to calculate the activation volume at different τ, from which we can estimate the corresponding incident dislocation length l_{inc} (i.e., the diameter of the semicircular saddle loop which is usually a few nanometers) involved in rebounding a new dislocation: $l_{\text{inc}} = 2[2(-\partial Q_0/\partial\tau)/(\pi a/\sqrt{3})]^{1/2}$, where a is the lattice constant. E_k is then evaluated for atoms inside the volume defined by l_{inc}, the core width, and core height [see the box in Fig. 3(b) and further explanation in Ref. [34]]. In Fig. 3(d), we see that $Q_0(\tau)$ and $E_k(\tau)$ intersect at $\tau \sim 1.45$ GPa, above which inequality (2) becomes satisfied. This critical τ for surface rebound to occur is consistent with the $\tau_{\text{reb}} \sim 1.4$ GPa, directly observed in our MD simulations. Figures 3(e) and 3(f) show the rebounded dislocation configurations under τ_{reb} and an initial temperature 2 K, which subsequently rose to ~12 K for a ~70 nm long incident dislocation. Viewed from the top [Fig. 3(e)] or bottom [Fig. 3(f)] in the direction along the dislocation line, the rebounded small dislocation loops alternate their locations from the upper layer to the lower layer, because near the critical τ_{reb} the E_k of the incident partial dislocation is sufficient to nucleate only one new partial, which emerges either above or below the original slip plane with apparently the same probability. Surface rebound was hypothesized by Frank [37] and Christian [38] before, but our MD simulations directly demonstrated it in a realistic metal and revealed its kinetic energy origin. Note that the typical artifacts associated with MD simulation of defect processes, those of unrealistically high applied strain rate and lack of rare-event sampling, are irrelevant here, since rebound arises only from an existing dislocation.

Next, we show that the SRS process is indeed the dominant mechanism to initiate DT in a copper nanowire, the sample geometry often used in laboratory experiments. The temporal correlation of dislocation dynamics in DT can be evaluated by the delay time t between two successive twinning dislocations, the nth after the $(n-1)$th. The shorter the t, the stronger the temporal correlation between the two. If the average t for SRS process t_{SRS} is significantly smaller than that of the TAN process t_{TAN}, i.e., $t_{\text{SRS}} \ll t_{\text{TAN}}$, then the SRS process would preempt the TAN. Here we evaluate the t_{SRS} by considering the travel distances and dislocation speeds for a 30 nm wide [100] oriented nanowire at 300 K. First, this nanowire is loaded under uniform compression to different σ levels at a strain rate of 10^8 s^{-1}. At each σ after relaxation, a small dislocation loop was introduced at one of the favored equivalent corners and accelerated to glide across the nanowire. By repeating such simulation under different σ,

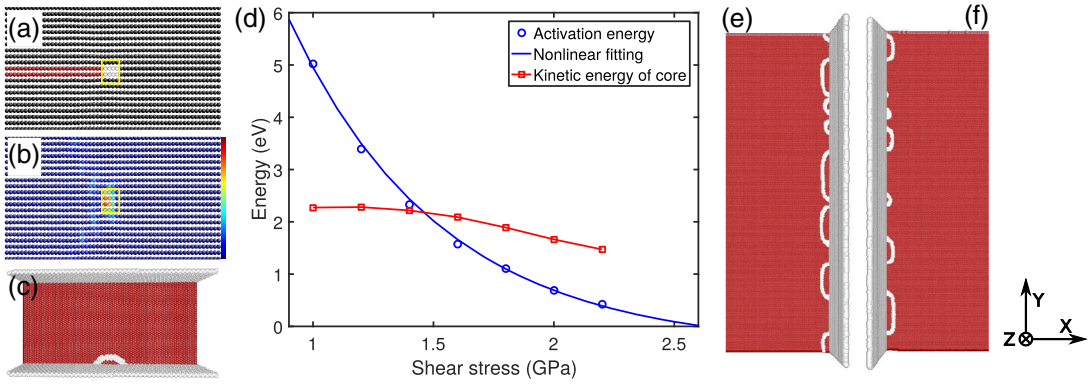

FIG. 3. Kinetic energy of the dislocation core induces free surface dislocation rebound. (a) The partial dislocation core (white atoms) identified by common neighbor analysis (CNA). (b) The core region (the yellow box) used in evaluating the kinetic energy. The color bar indicates the atomic kinetic energy range from 0 (blue) to 0.056 eV (red). (c) The saddle configuration of a twinning dislocation. The imposed shear stress τ in (a)–(c) is 1.6 GPa. (d) The kinetic energy of the dislocation core and the activation energy of twinning dislocation nucleation. (e)–(f) The rebounded dislocation loops of a ~70 nm long incident partial dislocation under the critical $\tau_{\text{reb}} = 1.4$ GPa at an initial temperature 2 K. The snapshots are taken at 1.3 ps after the impact. (a) and (b) share the same coordinate system: $X[1\bar{1}0]$, $Y[\bar{1}\,\bar{1}\,\bar{1}]$, and $Z[\bar{1}\,\bar{1}\,2]$. Coordinate systems in (c),(e), and (f) are $X[11\bar{2}]$, $Y[\bar{1}10]$, $Z[\bar{1}\,\bar{1}\,\bar{1}]$; $X[1\bar{1}0]$, $Y[\bar{1}\,\bar{1}\,2]$, $Z[111]$; and $X[\bar{1}10]$, $Y[\bar{1}\,\bar{1}\,2]$, $Z[\bar{1}\,\bar{1}\,\bar{1}]$, respectively. Atoms in (c), (e), and (f) are colored according to CNA. Red atoms represent stacking faults or twin boundaries, atoms on dislocation cores or free surfaces are white, and perfect FCC atoms are black.

the critical speed and axial stress for rebound in this nanowire was estimated to be $v_c \sim 0.60 c_t$ and $\sigma_{\text{reb}} \sim 1.5$ GPa, respectively. See Ref. [39] for typical rebound around the critical σ. Then t_{SRS} was estimated via dividing the characteristic sample length D (dislocation travel distance between two successive rebounds) by the dislocation speed v. This is because the frequency for SRS dislocations to hit the surface is very high in the nanoscale sample ($\sim 10^{10}$ s^{-1}, estimated from $v_c/10^2$ nm), and there is no time delay at the surfaces since Q is overcome entirely by E_k. The range of t_{SRS} (yellow band) by taking $v_c < v(\tau) < c_t$ and 10 nm $< D <$ 100 nm is shown in Fig. 4(a).

In comparison, for the TAN process the rate takes an Arrhenius form. Thus t_{TAN} can be calculated from the nucleation rate based on the activation free energy barrier Q. Here, $Q_0(\sigma)$ was FENEB calculated on the zero-T potential energy surface for the first six partial dislocations in a smaller ($\sim$5 nm wide) nanowire under different σ (see Ref. [40] for details). $Q(T) = (1 - T/T^*)Q_0(\sigma)$ [11] gives the value at $T = 300$ K, where $T^* = 700$ K is the approximate surface disordering temperature. t_{TAN} is then calculated according to $t_{\text{TAN}} = (\nu N)^{-1} \exp(Q/kT)$, where ν is the attempt frequency (3.0×10^{11} s^{-1}), N the total number of nucleation sites, and k the Boltzmann constant.

The results are shown in Fig. 4(a). In the limiting case where σ is so high that it overcomes the Q, TAN approaches the athermal limit such that the t_{TAN} of each partial becomes comparable with, or even shorter than, t_{SRS}. That is, when the σ level is initially very high prior to dislocation nucleation, TAN events could be too rampant on sample surfaces to leave any chance for the SRS process to operate. In our case, this happens [see the crossover in Fig. 4(a) of the t_{SRS} band with the t_{TAN} of the first couple of partial dislocations that initiate DT] when the axial stress $\sigma_{\text{ath}} \sim 2.75$ GPa at $T = 300$ K, well above that needed for rebound to occur ($\sigma_{\text{reb}} \sim 1.5$ GPa). As such, a wide stress window $[\sigma_{\text{reb}}, \sigma_{\text{ath}}]$ exists, where $t_{\text{SRS}} \ll t_{\text{TAN}}$. In this regime, the SRS dislocations easily preempt TAN due to their extraordinary temporal correlation. The $t_{\text{TAN}}(\sigma)$ curve would shift to the left with increasing twin thickness, but the driving stress level also gradually decreases such that the t_{TAN} remains well above t_{SRS}.

Figure 4(b) displays the axial stress σ_{p1} needed to nucleate the first dislocation via TAN, predicted based on the Q used in Fig. 4(a) at $T = 300$ K (see Ref. [41] for details of the calculation). The stress regime $[\sigma_{\text{reb}}, \sigma_{\text{ath}}]$ discussed above is indicated by the dashed lines. For normally accessible strain rates (from laboratory strain rate 10^{-3} s^{-1} to MD strain rates 10^8 s^{-1}), σ_{p1} almost perfectly falls into the stress window $[\sigma_{\text{reb}}, \sigma_{\text{ath}}]$, suggesting that when the first TAN event starts, the stress level is already sufficiently high for the SRS twinning dislocations to readily take over the subsequent DT initiation. This is consistent with our direct MD simulation shown in Fig. 1 where $\sigma_{p1} \sim 2.5$ GPa under the strain rate of 10^6 s^{-1} and DT is initiated completely by SRS twinning dislocations. On the contrary, as shown in Ref. [42], when a

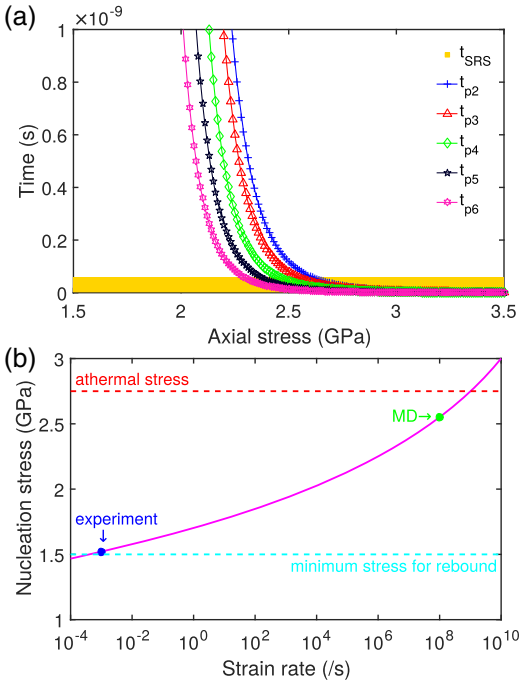

FIG. 4. Determination on the dominant mechanism underlying the strongly correlated DT initiation. (a) Delay time (or the temporal correlation) between successive dislocations. (b) The nucleation axial stress of the first dislocation via TAN at 300 K for normally accessible strain rates (as marked in the figure, 10^{-3} s^{-1} is typical for the strain rates used in laboratories, and 10^8 s^{-1} is often the strain rate applied in MD simulations), the predicted nucleation axial stress falls in the range of [1.5 GPa, 2.75 GPa] within which $t_{\text{SRS}} \leq t_{\text{TAN}}$.

50 nm NW is compressed under a much higher strain rate 10^9 s^{-1} at $T = 300$ K, σ_{p1} now becomes $\sim$3.0 GPa and TAN overwhelmingly dominates DT initiation. The above SRS dominated twinning stress window, on the order of 10^{-2} G, is encountered in laboratory experiments on most nanoscale metals such as Au [2,4], Cu [1,26,43], Al [44], Pd [3,5,45], and Ni [46], where the sample-level σ reported to nucleate the first dislocation is usually well in excess of 10^{-2} G, in the so-called ultra-strength regime [47,48]. We therefore conclude that SRS twinning dislocations constitute the preferred mechanism over TAN to initiate DT in typical small-volume experiments.

In summary, partial dislocations nucleated on the surface of pristine crystals can be accelerated by high stresses to approach the speed of the shear wave within a distance as short as 10^1 nm, and "bounce" back at free surfaces as twinning dislocations, directly initiating DT in a highly correlated, domino cascade manner. We confirmed that such surface rebound is a consequence of a strongly overdriven dislocation core carrying sufficiently high kinetic energy to overcome the static nucleation energy barrier of new dislocations. From the delay time to generate the next twinning dislocation, the surface rebound mechanism is significantly more probable than the TAN process under the same loading conditions. For a wide range of strain rates, the

nucleation stress of the first partial dislocation in metallic nanowires is well beyond the minimum stress required for surface rebound. These render the surface rebound mechanism highly efficient and preferable. As such, in an experimentally relevant stress window, SRS relay dominates over TAN for DT initiation. This affirms the nature of DT to be "stimulated slip," and its strongly correlated kinetics *vis-à-vis* ordinary dislocation slip is akin to "what laser (light amplification by stimulated emission of radiation) is to normal light" [49]. In DT-SRS the stimulation is of kinetic energy origin, whereas in DT-TAN (below σ_{reb} or above σ_{ath}) the stimulation is of configurational energy origin.

Note that a nanoscale pristine crystal is only one example that is amenable to the operation of surface rebound. The mechanism demonstrated here may also have relevance to high-stress or high-strain-rate deformation in general, where strongly overdriven dislocations interact with interfaces. For example, DT in bulk nanocrystalline metals relies on partials nucleated from grain boundaries under high stresses to run towards opposing boundaries at high speeds. In shock loading, the shock width is too small to include many dislocation sources, such that high-speed dislocation interacting with large voids [50] or phase boundaries [51] may come into play to multiply dislocations.

Q. J. L. and E. M. were supported by U.S.-DOE-BES-DMSE, DE-FG02-09ER46056. J. L. acknowledges support by NSF Grant No. DMR-1410636. Z. W. S. was supported by NSFC Grants No. 51231005, No. 51321003 and the International Joint Laboratory for Micro/Nano Manufacturing and Measurement Technologies.

*Corresponding authors.
liju@mit.edu
†zwshan@mail.xjtu.edu.cn
‡ema@jhu.edu

[1] G. Richter, K. Hillerich, D. S. Gianola, R. Mönig, O. Kraft, and C. A. Volkert, Nano Lett. **9**, 3048 (2009).
[2] J.-H. Seo *et al.*, Nano Lett. **11**, 3499 (2011).
[3] L. Y. Chen, G. Richter, J. P. Sullivan, and D. S. Gianola, Phys. Rev. Lett. **109**, 125503 (2012).
[4] A. Sedlmayr, E. Bitzek, D. S. Gianola, G. Richter, R. Mönig, and O. Kraft, Acta Mater. **60**, 3985 (2012).
[5] J.-H. Seo, H. S. Park, Y. Yoo, T.-Y. Seong, J. Li, J.-P. Ahn, B. Kim, and I.-S. Choi, Nano Lett. **13**, 5112 (2013).
[6] B. Roos, B. Kapelle, G. Richter, and C. A. Volkert, Appl. Phys. Lett. **105**, 201908 (2014).
[7] L. Y. Chen, M.-r. He, J. Shin, G. Richter, and D. S. Gianola, Nat. Mater. **14**, 707 (2015).
[8] See Supplemental Material at http://link.aps.org/supplemental/10.1103/PhysRevLett.117.165501, Fig. S1, for the schematic of strongly correlated deformation twinning initiation process, which includes Refs. [2, 4–6].
[9] A. H. Cottrell and B. A. Bilby, Philos. Mag. **42**, 573 (1951).
[10] N. Thompson and D. J. Millard, Philos. Mag. **43**, 422 (1952).
[11] T. Zhu, J. Li, A. Samanta, A. Leach, and K. Gall, Phys. Rev. Lett. **100**, 025502 (2008).
[12] C. R. Weinberger, A. T. Jennings, K. Kang, and J. R. Greer, J. Mech. Phys. Solids **60**, 84 (2012).
[13] A. T. Jennings, C. R. Weinberger, S.-W. Lee, Z. H. Aitken, L. Meza, and J. R. Greer, Acta Mater. **61**, 2244 (2013).
[14] T. Zhu, J. Li, A. Samanta, H. G. Kim, and S. Suresh, Proc. Natl. Acad. Sci. U.S.A. **104**, 3031 (2007).
[15] Y. Mishin, M. J. Mehl, D. A. Papaconstantopoulos, A. F. Voter, and J. D. Kress, Phys. Rev. B **63**, 224106 (2001).
[16] S. Plimpton, J. Comput. Phys. **117**, 1 (1995).
[17] J. Li, Model. Simul. Mater. Sci. Eng. **11**, 173 (2003).
[18] A. Stukowski and K. Albe, Model. Simul. Mater. Sci. Eng. **18**, 085001 (2010).
[19] See Supplemental Material at http://link.aps.org/supplemental/10.1103/PhysRevLett.117.165501, section II, for more details on simulation methods, which includes Ref. [20].
[20] M. Parrinello and A. Rahman, J. Appl. Phys. **52**, 7182 (1981).
[21] See Supplemental Material at http://link.aps.org/supplemental/10.1103/PhysRevLett.117.165501, Fig. S2, for the stress vs time curve for the 10 nm wide nanowire being compressed.
[22] See Supplemental Material at http://link.aps.org/supplemental/10.1103/PhysRevLett.117.165501, movie 1, for the surface rebound sustained deformation twinning initiation as discussed in Fig. 1 in text.
[23] See Supplemental Material at http://link.aps.org/supplemental/10.1103/PhysRevLett.117.165501, movie 2, for surface rebound dominated DT initiation in a 10 nm wide [110] oriented nanowire under tensile loading.
[24] L. O. David, G. H. Louis, Jr., W. A. Curtin, and R. J. Clifton, Model. Simul. Mater. Sci. Eng. **13**, 371 (2005).
[25] P. Gumbsch and H. Gao, Science **283**, 965 (1999).
[26] D. Kiener and A. M. Minor, Nano Lett. **11**, 3816 (2011).
[27] See Supplemental Material at http://link.aps.org/supplemental/10.1103/PhysRevLett.117.165501, Fig. S3, for a dislocation acceleration process at 300 K.
[28] J. D. Eshelby, Proc. Phys. Soc. London Sect. A **62**, 307 (1949).
[29] F. C. Frank, Proc. Phys. Soc. London Sect. A **62**, 131 (1949).
[30] J. Weertman, in *Response of Metals to High Velocity Deformation*, edited by P. G. Showmon and V. F. Zackay (Interscience, New York, Colorado, 1961), p. 205.
[31] J. Hirth and J. Lothe, *Theory of Dislocations*, 2nd ed. (John Wiley & Sons, New York, 1982).
[32] D. Faken and H. Jónsson, Comput. Mater. Sci. **2**, 279 (1994).
[33] H. Tsuzuki, P. S. Branicio, and J. P. Rino, Comput. Phys. Commun. **177**, 518 (2007).
[34] See Supplemental Material at http://link.aps.org/supplemental/10.1103/PhysRevLett.117.165501, Fig. S4, Fig. S5, Fig. S6 and associated discussions, for the underlying physics for choosing the core region to calculate the effective kinetic energy during the surface rebound process.
[35] See Supplemental Material at http://link.aps.org/supplemental/10.1103/PhysRevLett.117.165501, section II and Fig. S7, for details on the free end nudged elastic band calculations, which includes Refs. [11,14,36].
[36] G. Henkelman and H. Jónsson, J. Chem. Phys. **111**, 7010 (1999).
[37] F. C. Frank, *Report of the Conference on Strength of Solids* (Physical Society, London, Bristol, 1948), p. 46.

[38] J. W. Christian, Proc. R. Soc. A **206**, 51 (1951).
[39] See Supplemental Material at http://link.aps.org/supplemental/10.1103/PhysRevLett.117.165501, Fig. S8, for typical DT initiation processes in a 30 nm nanowire with axial stress around the critical value for surface rebound.
[40] See Supplemental Material at http://link.aps.org/supplemental/10.1103/PhysRevLett.117.165501, section II and Fig. S9, for details on free end nudged elastic band calculations on the activation energies of the first six partial dislocations during deformation twinning initiation in a nanowire.
[41] See Supplemental Material at http://link.aps.org/supplemental/10.1103/PhysRevLett.117.165501, section II, for more details on the nucleation stress calculations.
[42] See Supplemental Material at http://link.aps.org/supplemental/10.1103/PhysRevLett.117.165501, movie 3, for thermally activated nucleation dominated deformation twinning initiation in a 50 nm wide nanowire compressed to near the athermal stress level.
[43] Y. Yue, P. Liu, Z. Zhang, X. Han, and E. Ma, Nano Lett. **11**, 3151 (2011).
[44] Z.-J. Wang, Q.-J. Li, Z.-W. Shan, J. Li, J. Sun, and E. Ma, Appl. Phys. Lett. **100**, 071906 (2012).
[45] L. Y. Chen, S. Terrab, K. F. Murphy, J. P. Sullivan, X. Cheng, and D. S. Gianola, Rev. Sci. Instrum. **85**, 013901 (2014).
[46] C. Peng, Y. Ganesan, Y. Lu, and J. Lou, J. Appl. Phys. **111**, 063524 (2012).
[47] T. Zhu and J. Li, Prog. Mater. Sci. **55**, 710 (2010).
[48] J. Li, Z. Shan, and E. Ma, MRS Bull. **39**, 108 (2014).
[49] Q. Yu, Z.-W. Shan, J. Li, X. Huang, L. Xiao, J. Sun, and E. Ma, Nature (London) **463**, 335 (2010).
[50] L. Xiong, S. Xu, D. L. McDowell, and Y. Chen, Int. J. Plast. **65**, 33 (2015).
[51] P. A. Pluchino, X. Chen, M. Garcia, L. Xiong, D. L. McDowell, and Y. Chen, Comput. Mater. Sci. **111**, 1 (2016).